

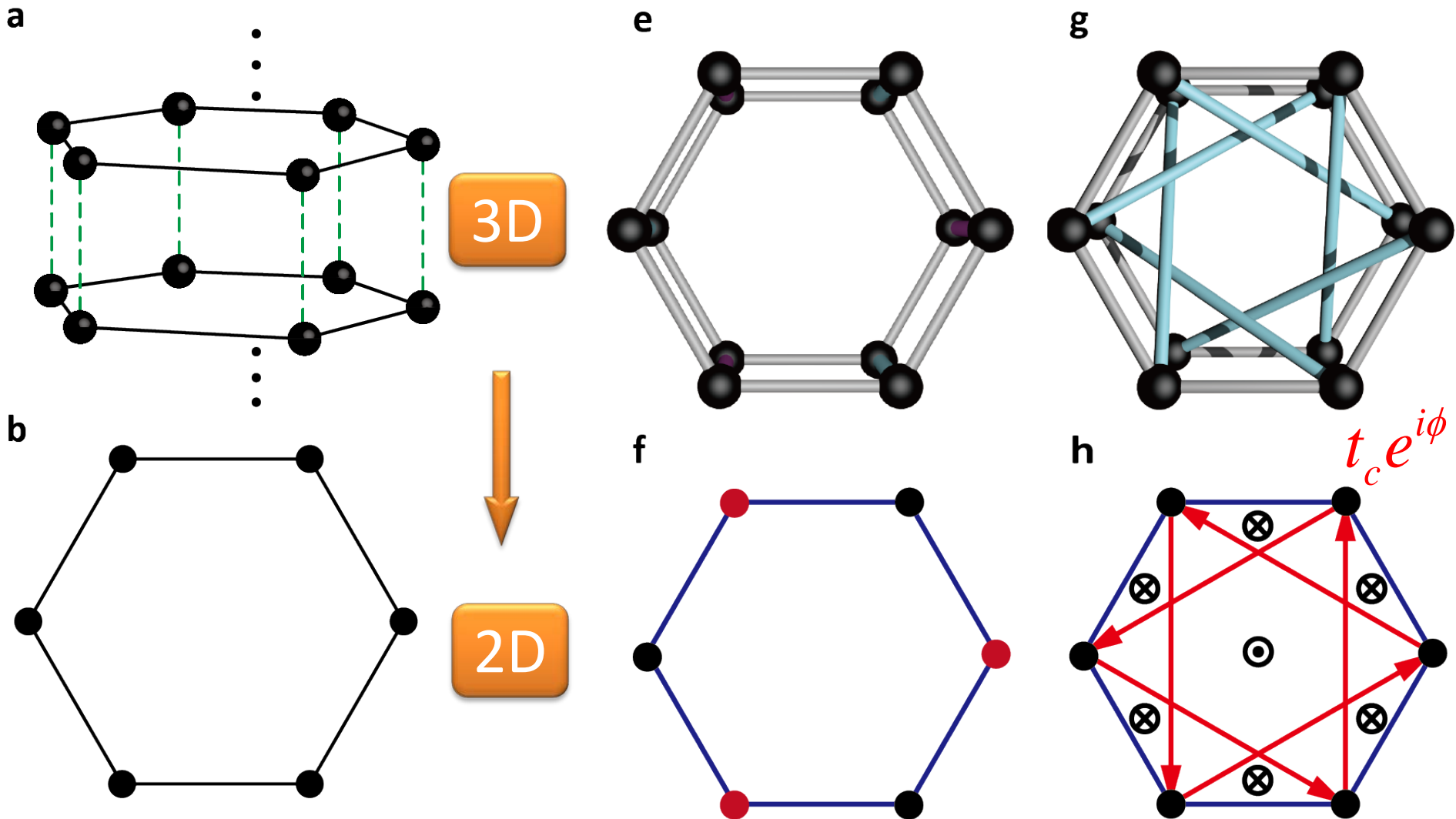
# Weyl Points and Topological Notions in Classical Waves

- **Synthetic gauge flux and Weyl points in acoustic systems**
- **Experimental observation of Robust surface states on Weyl photonic crystals**
- **Symmetry-protected transport in a pseudospin-polarized waveguide**

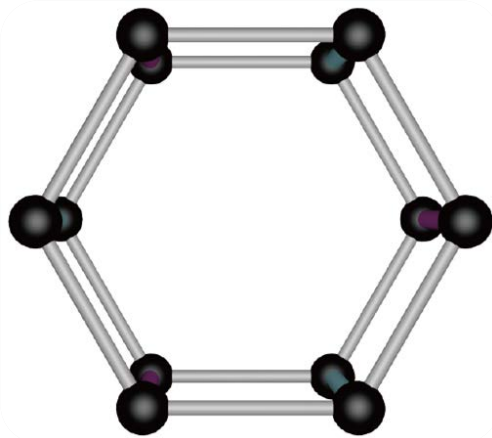
Acknowledgement: Hong Kong Research Grants Council (Grant No. AoE/P-02/12)



# Haldane Model realized with interlayer coupling engineering



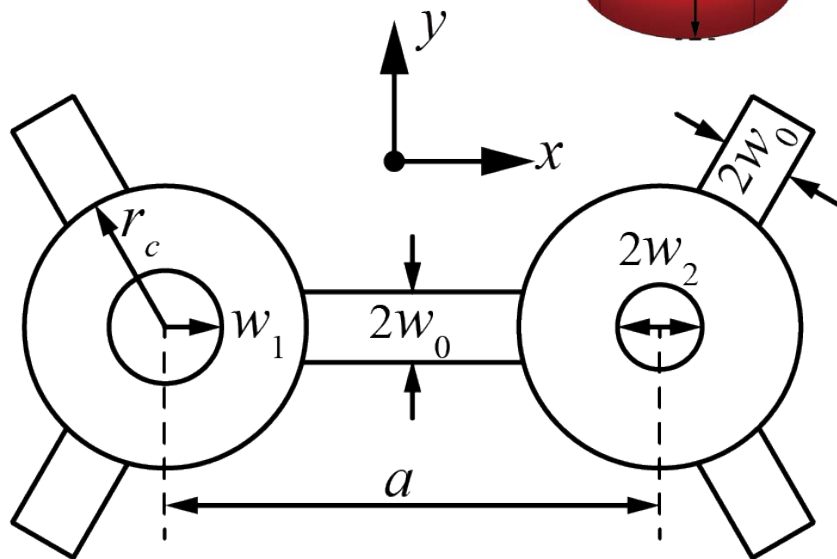
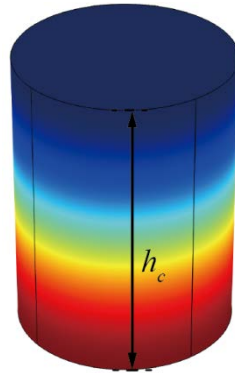
# inversion symmetry breaking



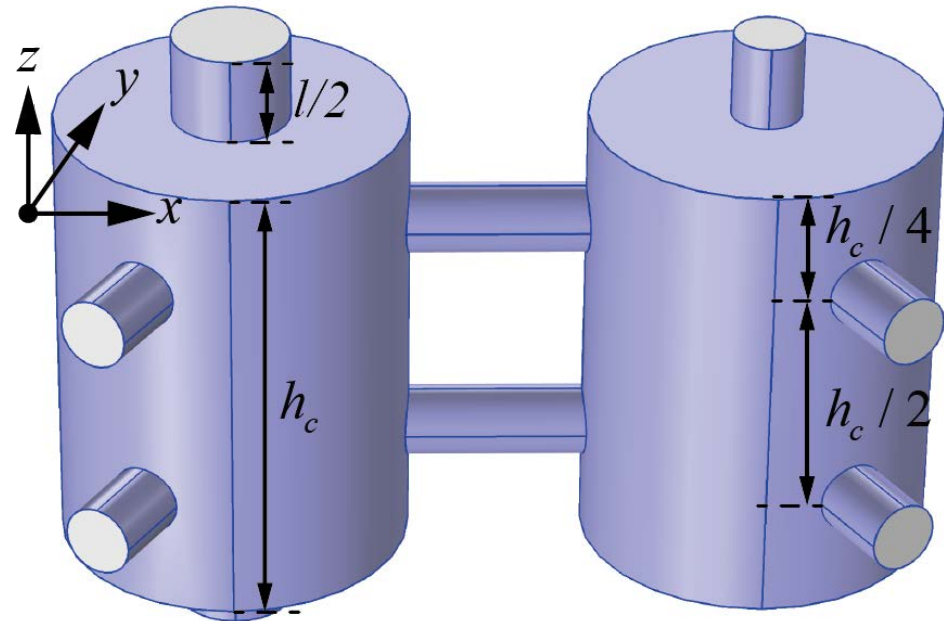
Atom



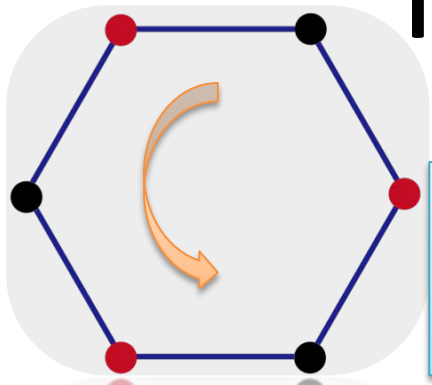
Resonance cavity



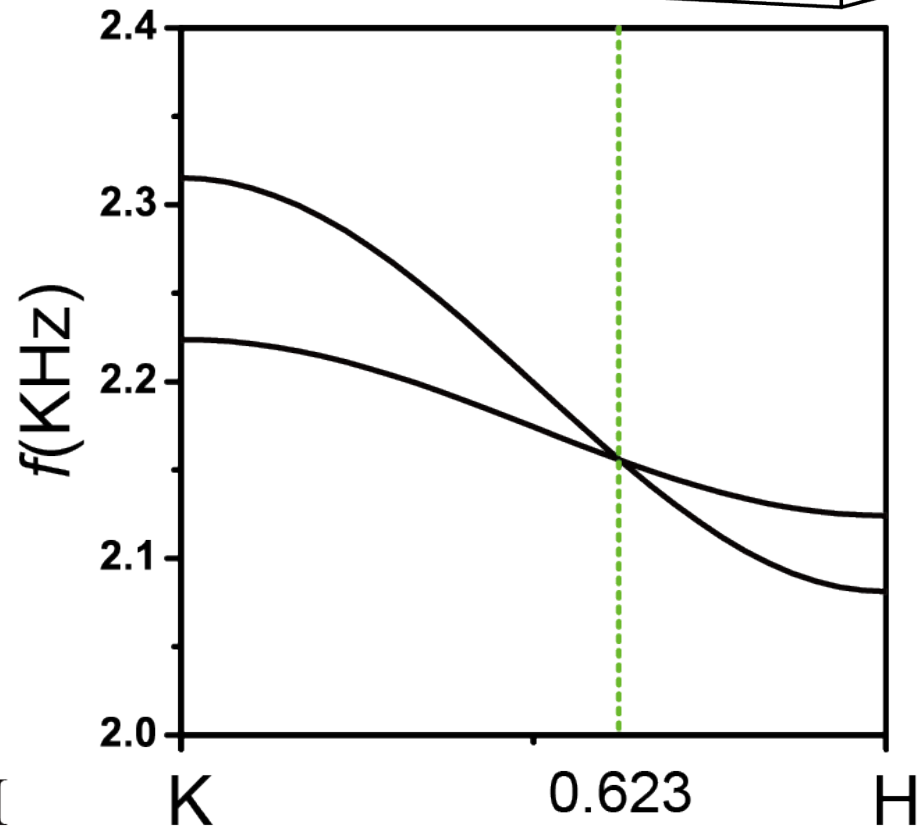
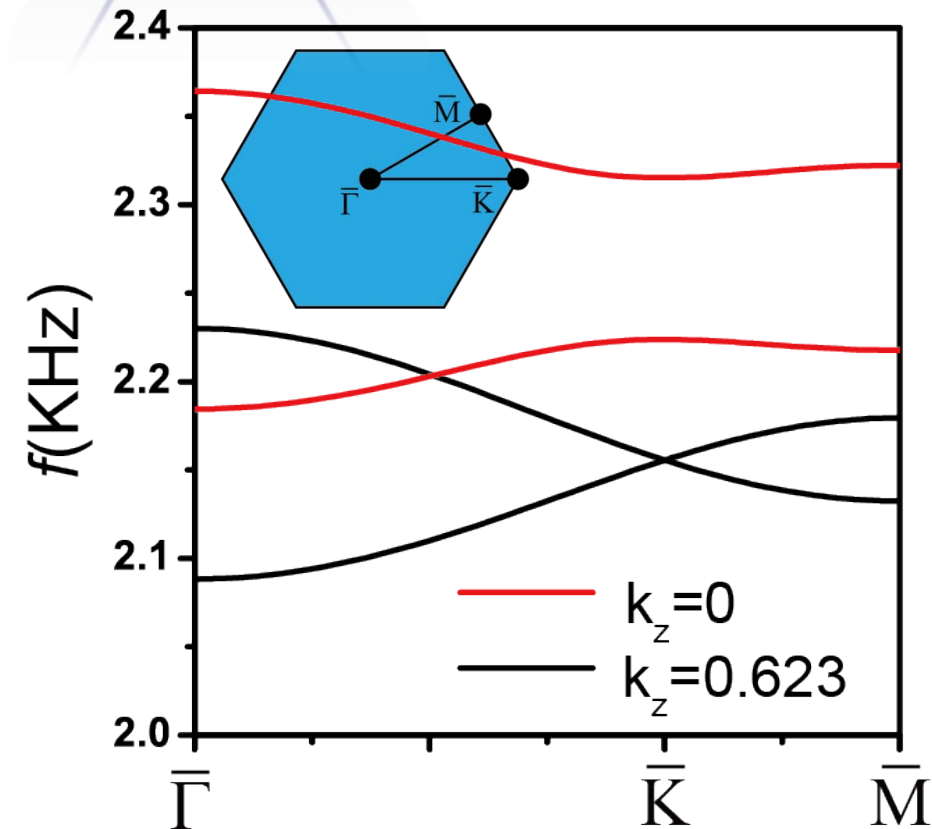
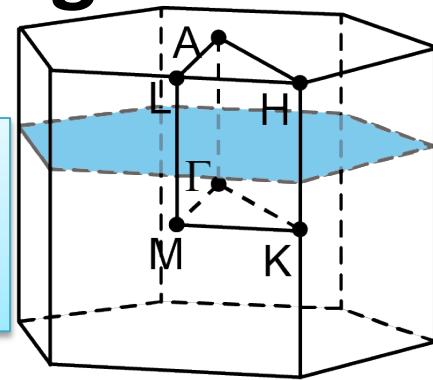
**Hopping** is realized with small connection **tubes** between atoms. Hopping **strength** is tuned with the **radius** ( $w$ ) of connection tubes,  $\propto w^2$  when  $w$  is not too large.

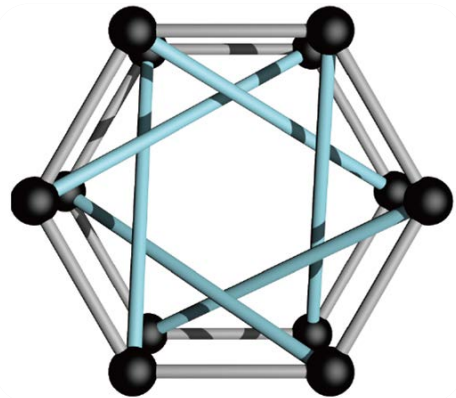


# inversion symmetry breaking



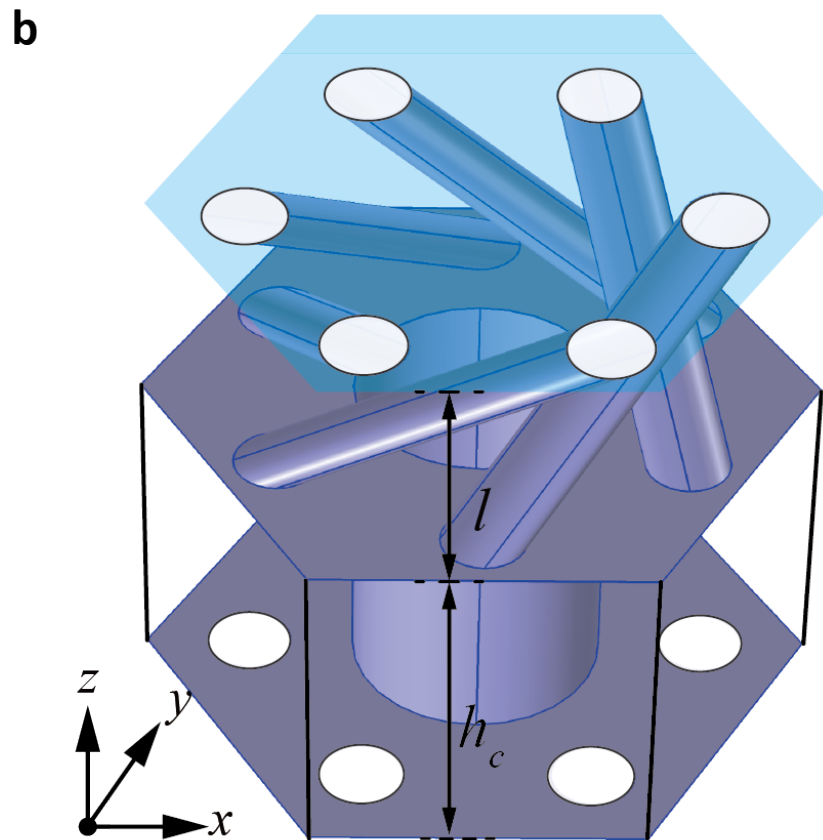
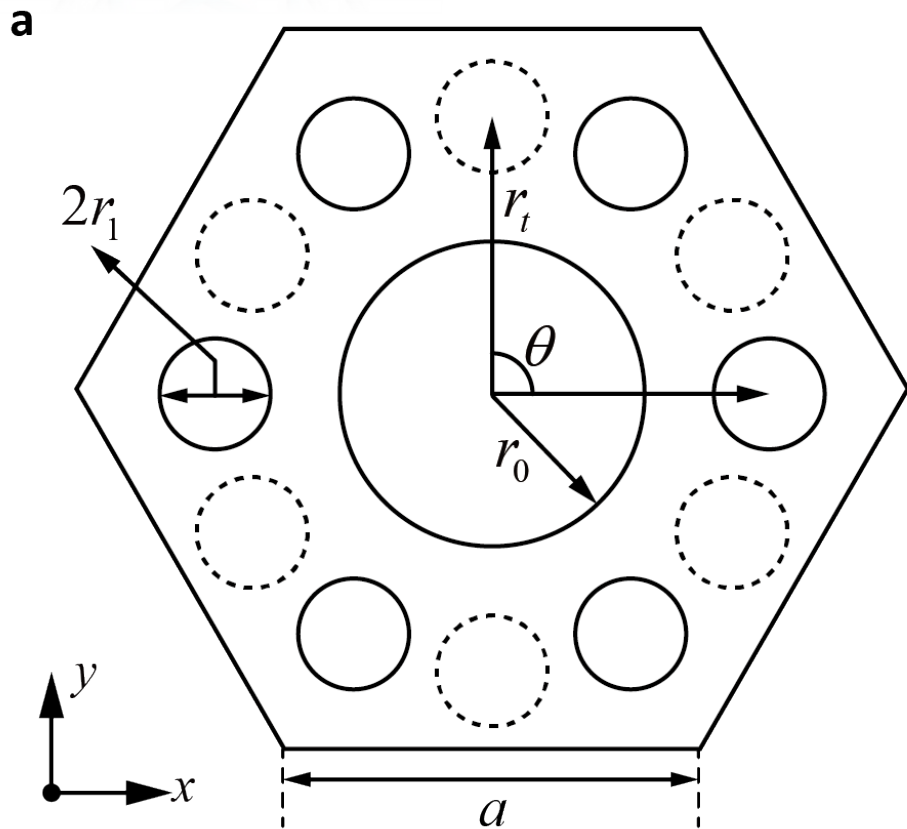
Inversion symmetry is broken at  $k_z \neq 0.623$   
Inversion symmetry breaking introduces  
trivial band with zero Chern number.



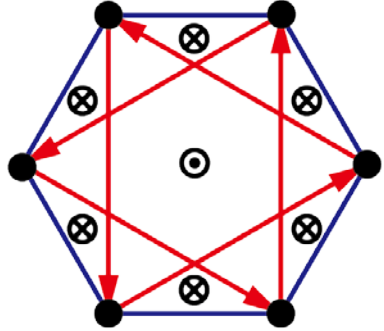


# Chiral Interlayer coupling

$$d_h = h_c + l$$

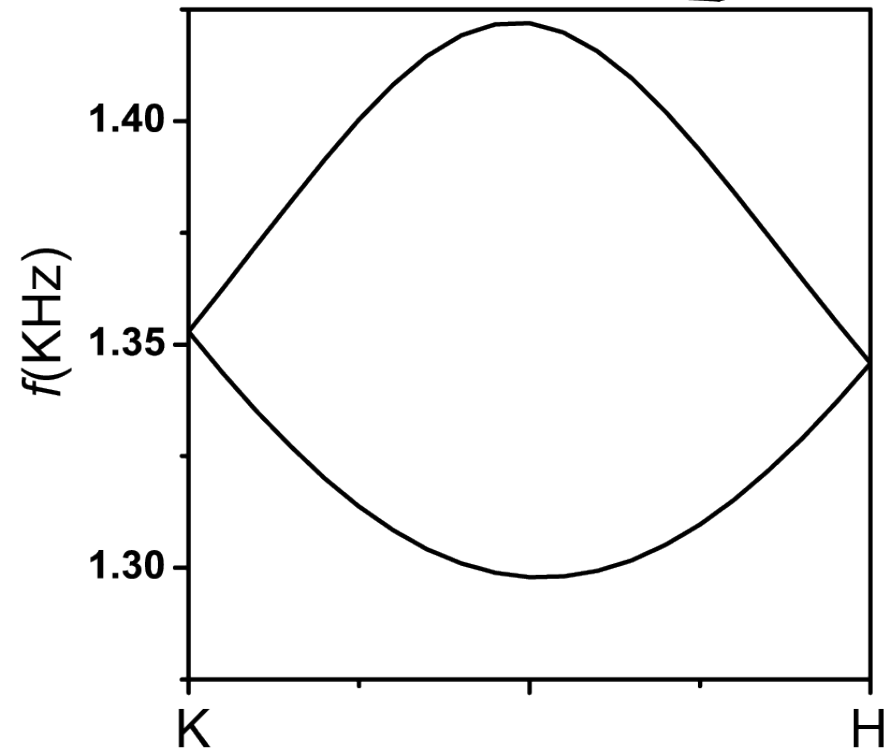
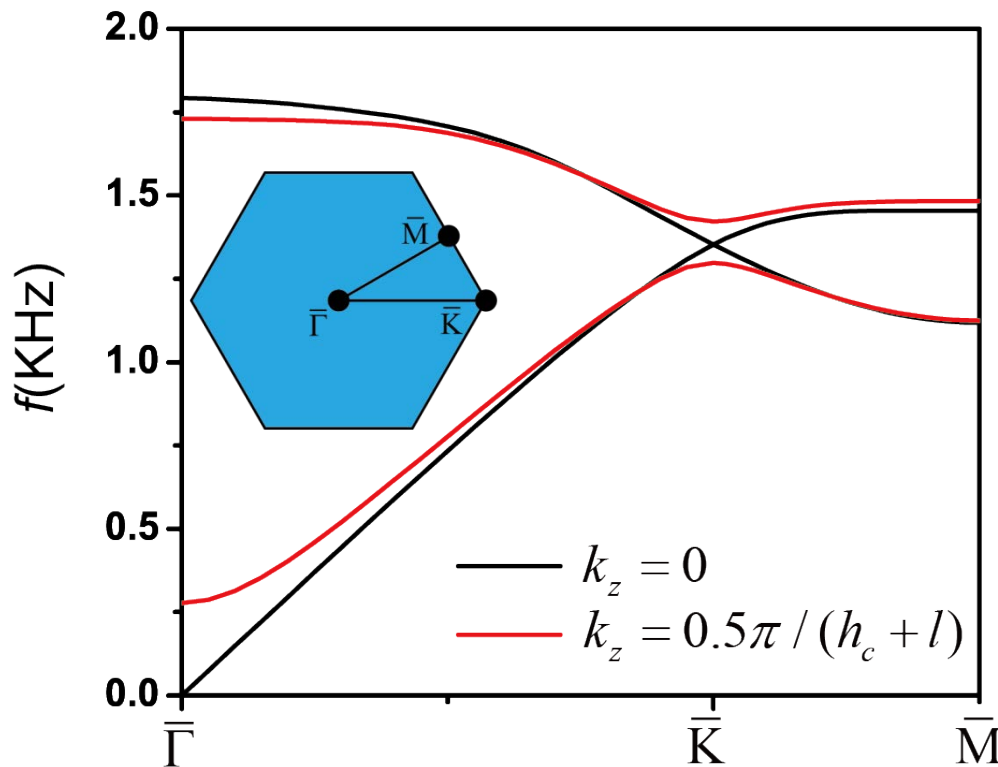
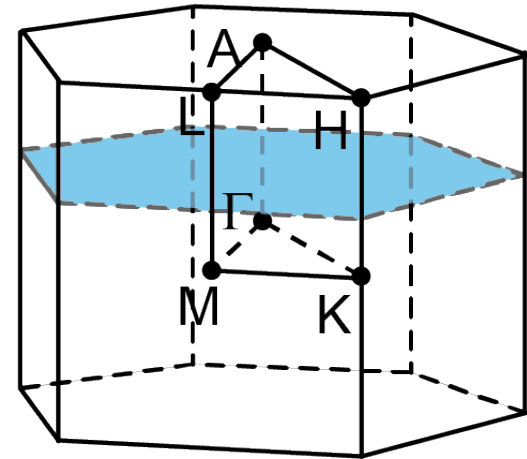


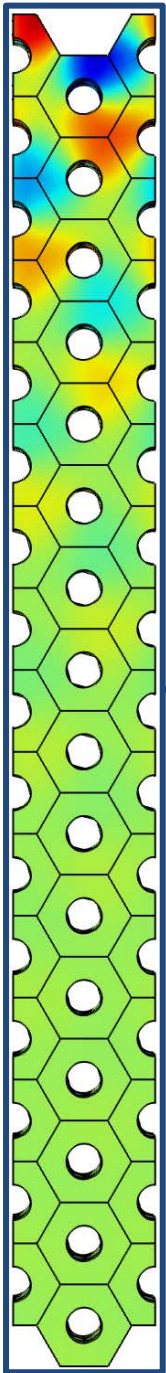
# Synthetic gauge flux



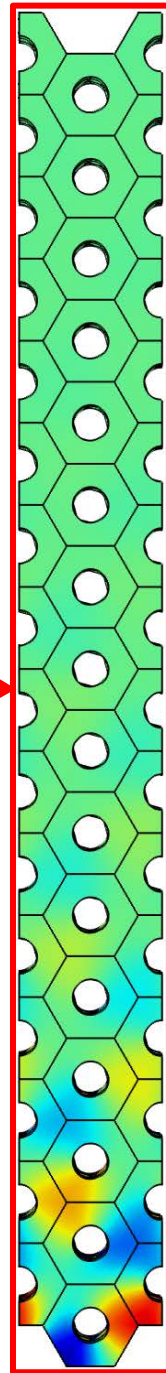
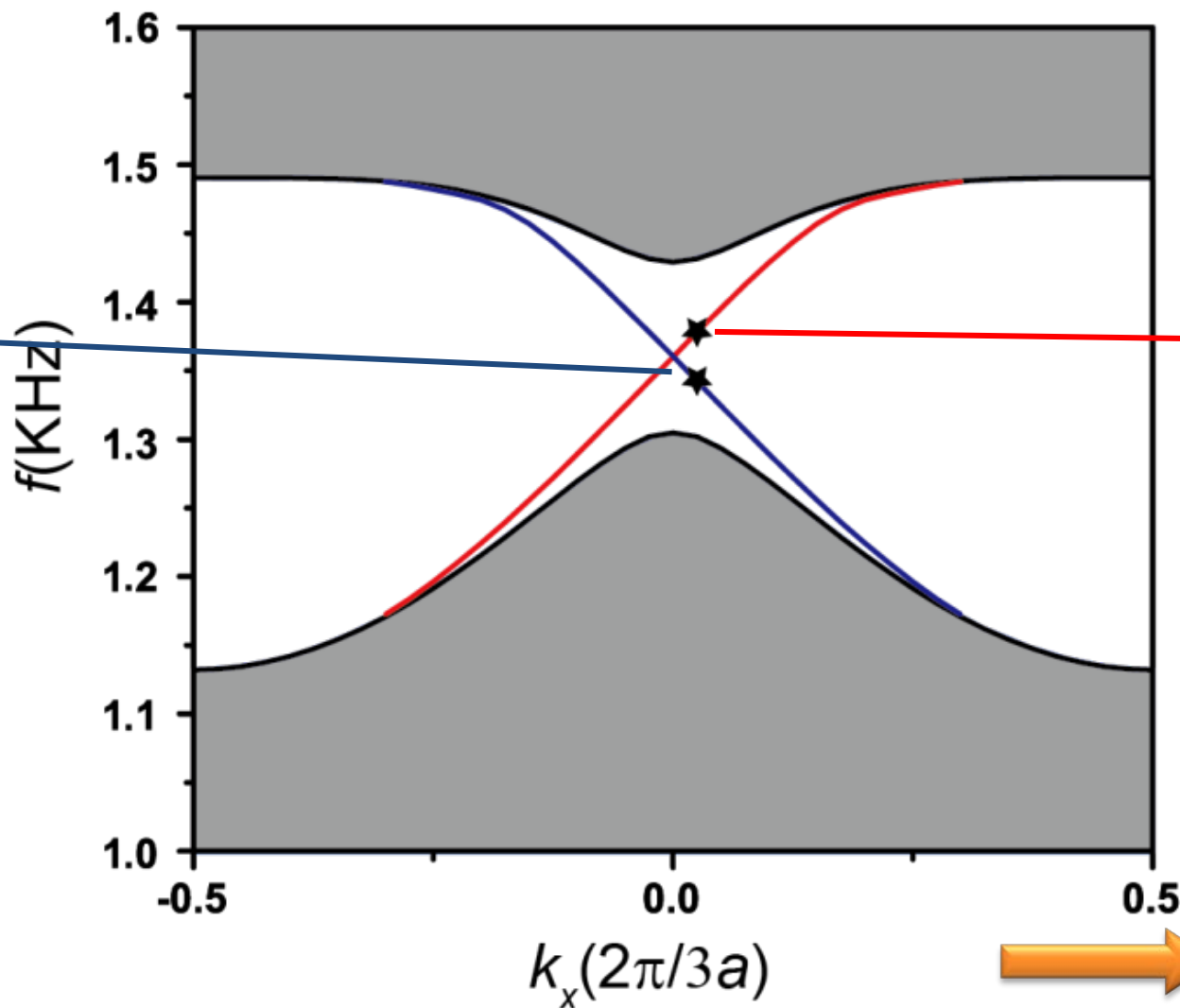
When  $k_z \neq 0, \pi$ , the Chern number of the lower band is  $\pm 1$ .

Sign of Chern number depends on the sign of  $k_z$ .





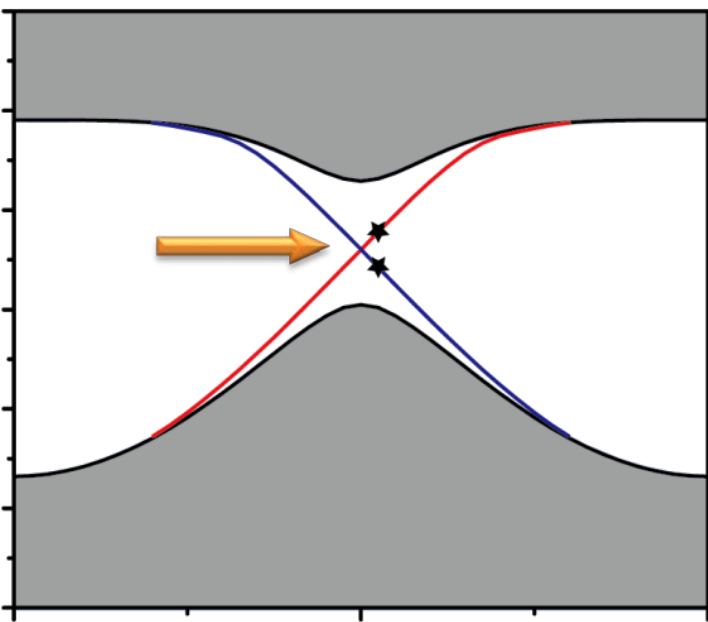
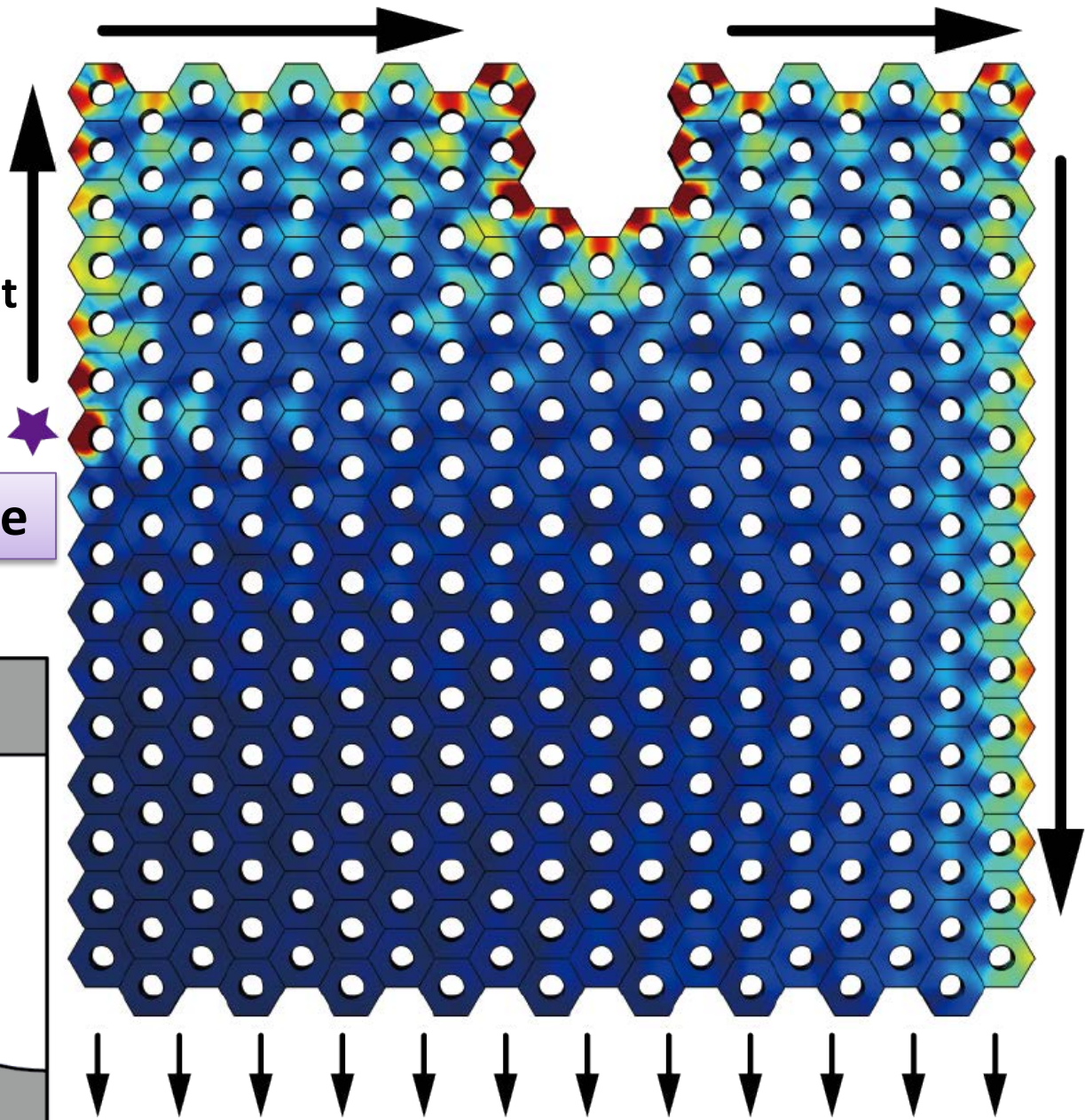
Projection band and one-way edge state at  $k_z = 0.5\pi / d_h$



# One Way edge mode

Acoustic wave propagates across corners and the defect without being backscattered as long as  $k_z$  is a good quantum number.

Source



# Weyl Point

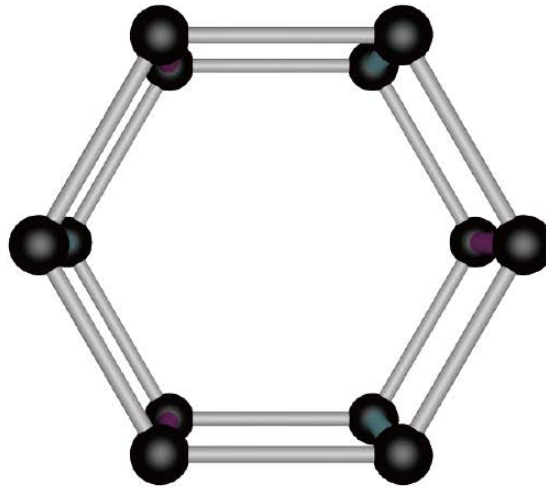
$$H(\mathbf{k}) = \sum k_i v_{ij} \sigma_j$$

$i, j \in \{x, y, z\}$ ,  $\sigma$  is Pauli matrix

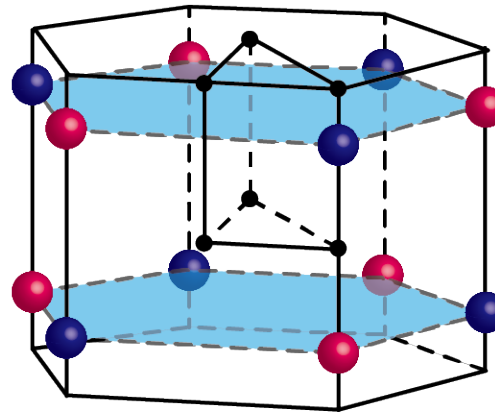
- Weyl have **chirality**, i.e., “charge”

$$c = \text{sgn}(\det[v_{ij}])$$

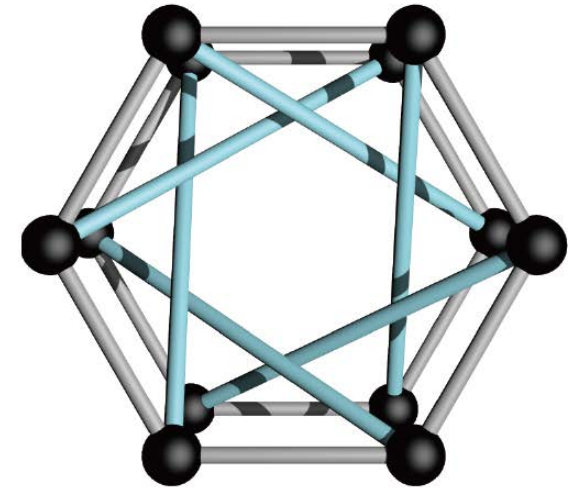
- Weyl points are topological defects, act as monopoles of Berry flux. Starts from positive charge, end at negative charge,
- Chern number of 2D band is related to Weyl point.



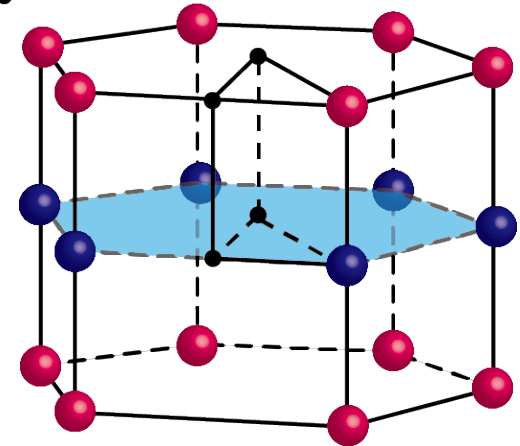
a



● Positive charge



b



● Negative charge

# Microwave Weyl photonic crystal

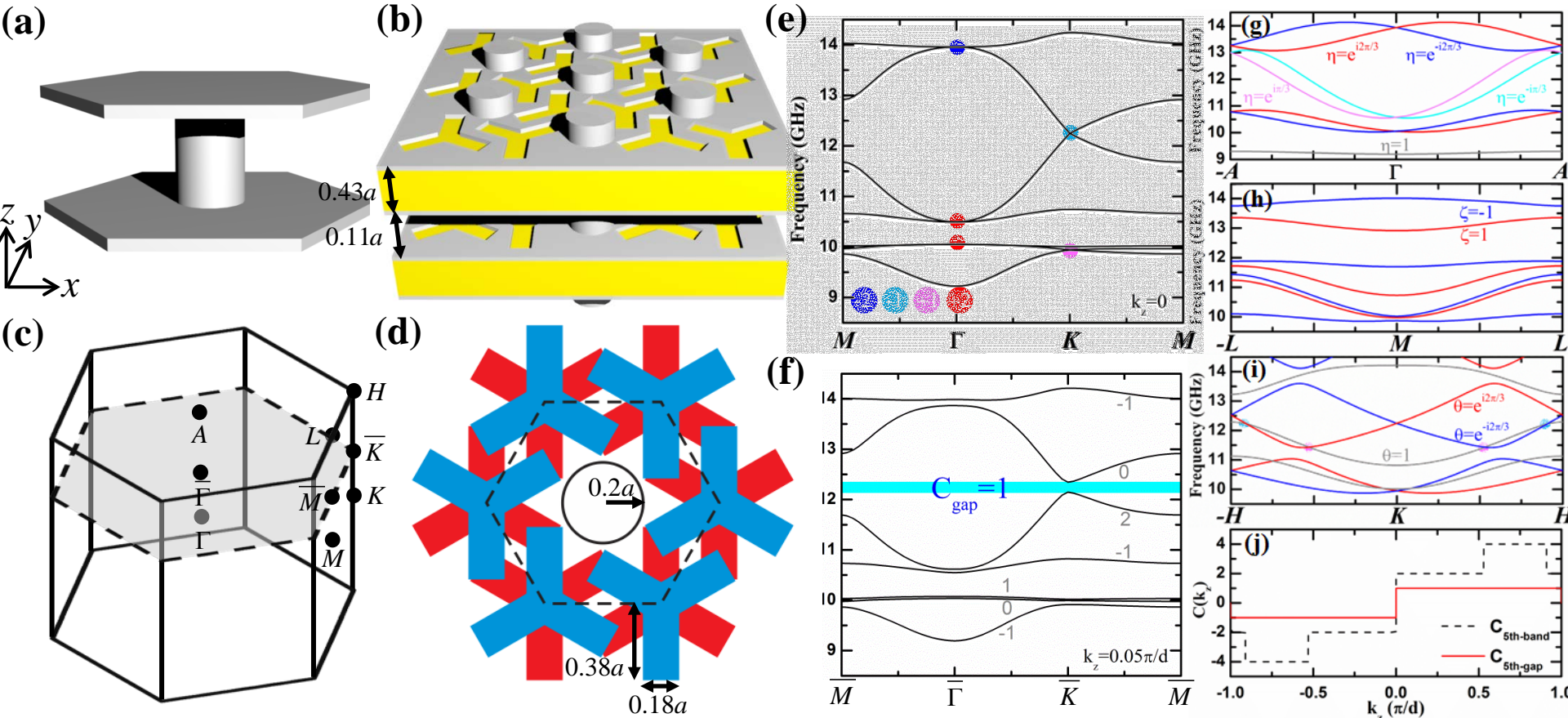


**Fig. 1. Realization of Weyl points in EM system by introducing interlayer coupling.** (a) The unit cell of a single layer system built from a hexagonal array of PEC cylinders bounded by two PEC slabs. (b) Multilayer system built from PCB boards stacked in  $z$ -direction. Interlayer couplings are introduced by the Y-shaped slots on both sides of the PCB boards. (c) Reciprocal space of the hexagonal lattice. (d) Top view of the unit cell (dashed hexagon) of multilayer system. Blue and red area highlight the Y-shaped slots on upper surface and lower surface of the PCB board. (e) Bulk band structure on the  $k_z=0$  plane. It has several Weyl points with different charges (highlighted by different colors). (f) Bulk band structure on the  $k_z = 0.05 \frac{\pi}{d}$  plane. (g) Bulk band structure on the  $k_z=0$  plane. It has several Weyl points with different charges (highlighted by different colors). (h) Bulk band structure on the  $k_z=0$  plane. It has several Weyl points with different charges (highlighted by different colors). (i) Bulk band structure on the  $k_z=0$  plane. It has several Weyl points with different charges (highlighted by different colors). (j) Chern number  $C(k)$  vs  $k_x (\pi/d)$  for the 5th band and 5th gap.

# Setup for bulk transmission measurement

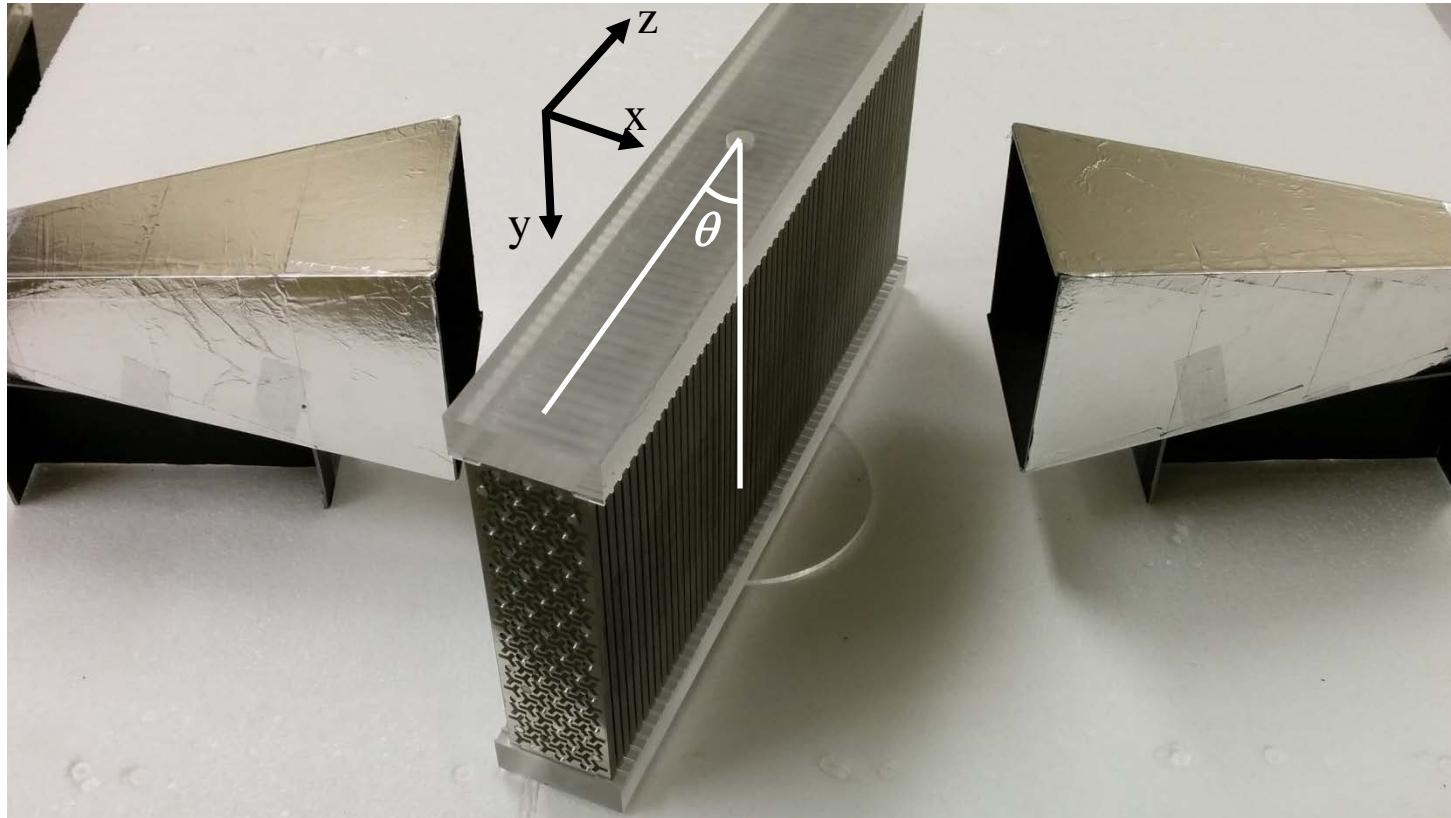


**Fig. 2. Experimental setup for measuring bulk transmission.** EM waves are emitted and received by two horn antennas with electric field lying in  $xz$  plane. By changing the incident angle  $\theta$ , bulk states with different  $k_z = 2\pi f \sin\theta / c$  can be excited.

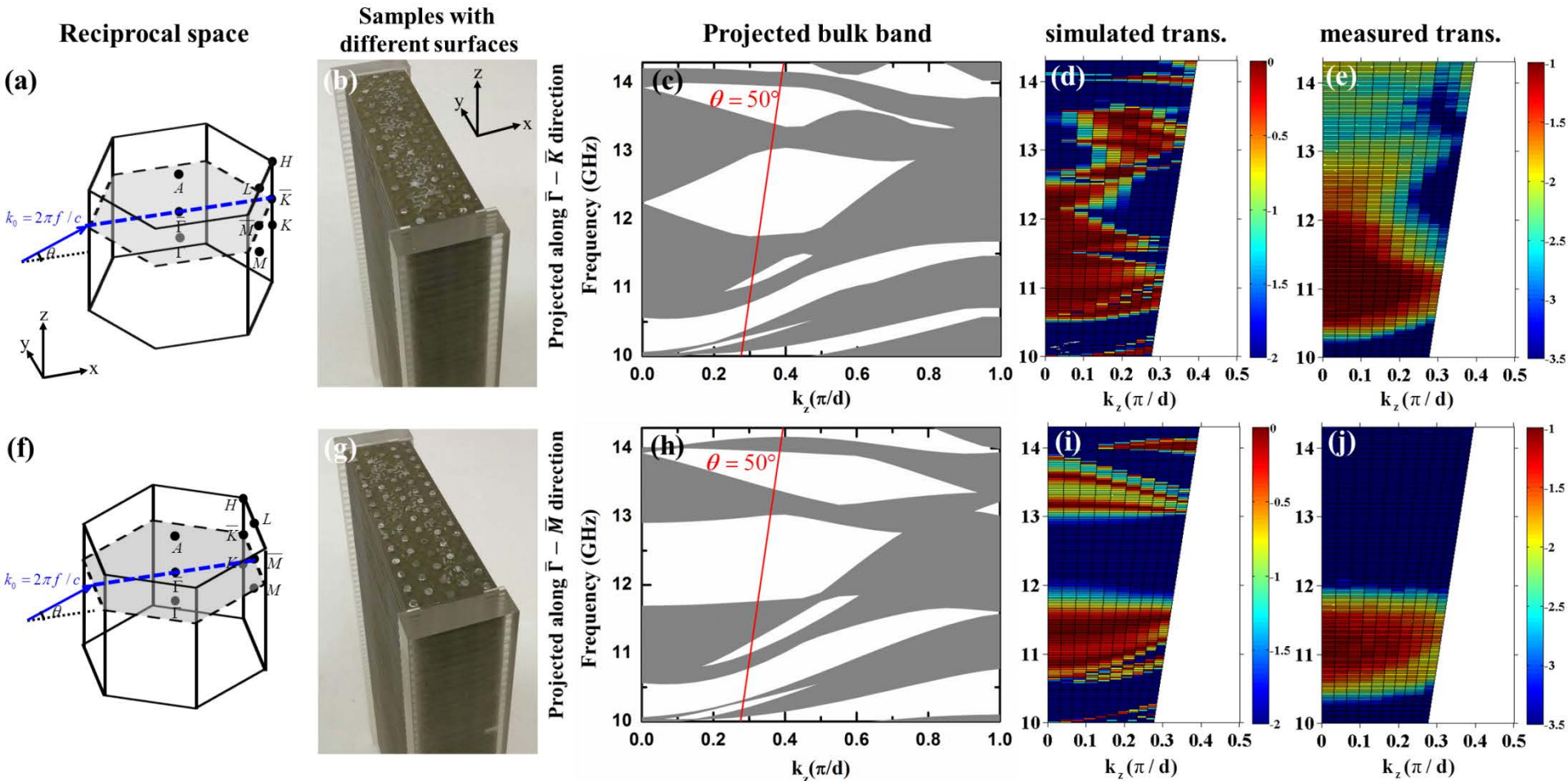


**Fig. 3. Projected band structure and bulk transmissions.** (a) Reciprocal space corresponding to the sample shown in (b). (b) Photograph of the sample with surface perpendicular to the  $\bar{\Gamma} - \bar{K}$  direction. Blue arrow in (a) indicates the wave vector of the incident wave with tilted angle  $\theta$ . The bulk modes lying at the blue dashed line, which is parallel to the  $\bar{\Gamma} - \bar{K}$  direction, can be excited. (c) Bulk band projected along the  $\bar{\Gamma} - \bar{K}$  direction as a function of  $k_z$ . (d)/(e) simulated and measured transmission spectra along the  $\bar{\Gamma} - \bar{K}$  direction. (f) Reciprocal space corresponding to the sample shown in (g). (g) Sample with surface perpendicular to the  $\bar{\Gamma} - \bar{M}$  direction. (h) Bulk band projected along the  $\bar{\Gamma} - \bar{M}$  direction. (i)/(j) simulated and measured transmission spectra along the  $\bar{\Gamma} - \bar{M}$  direction.

# Calculated surface dispersion between Weyl photonic crystal and PEC

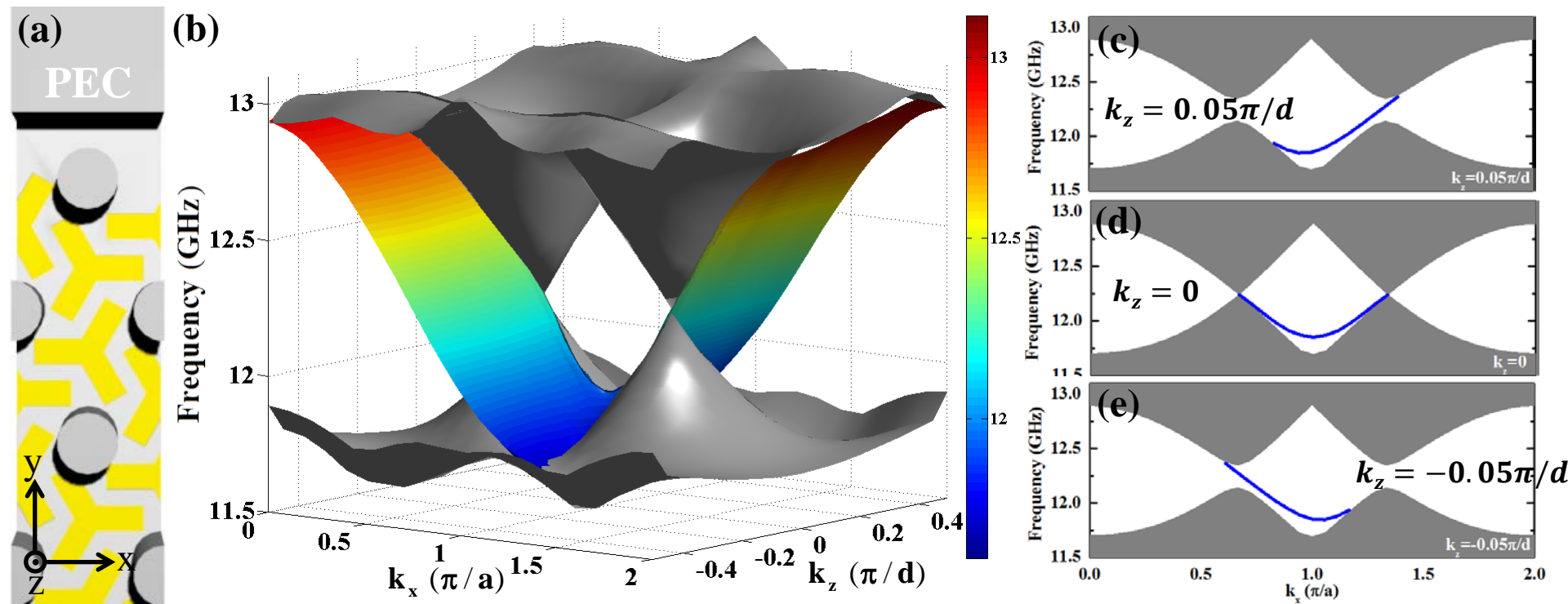
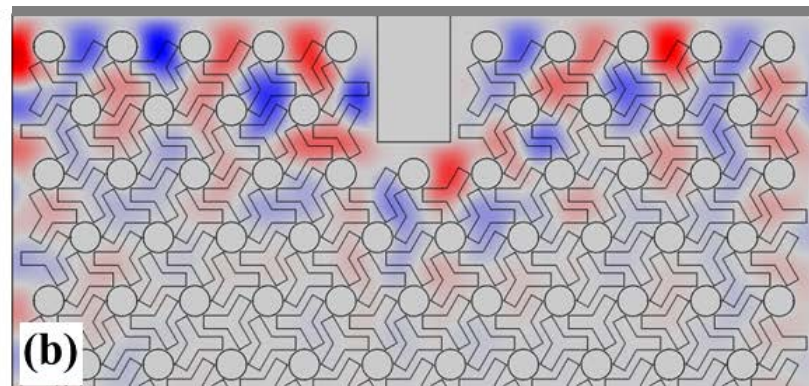
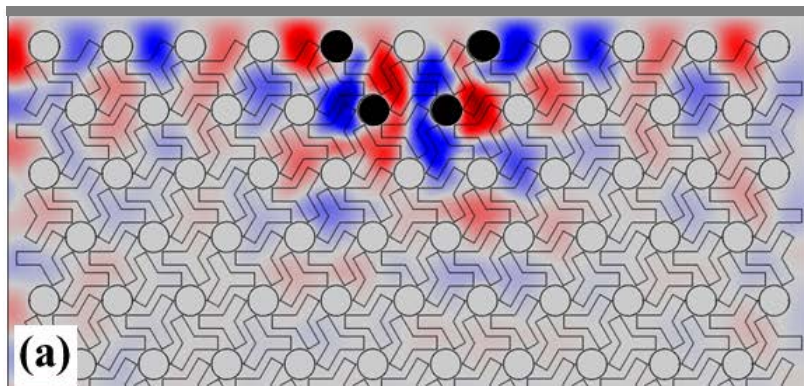


**Fig. 4. Surface dispersion between Weyl photonic crystal and PEC.** (a) Configuration of the Weyl photonic crystal bounded by a PEC slab. (b) Calculated surface dispersion in the surface Brillouin zone. For clarity, only half of the Brillouin zone ( $k_z \in [-0.5\frac{\pi}{d}, 0.5\frac{\pi}{d}]$ ) is plotted. Projected bulk states are plotted in gray while the surface states are plotted in color. Two linear cones of bulk states lying at  $k_z=0$  plane are due to the two Weyl points at K and K' with topological charge of -1. The two Weyl points at H and H' with charge of +1, which lie at  $k_z=\pi$  plane, are not shown. (c)-(e) Surface dispersions at  $k_z = 0.05\frac{\pi}{d}$ ,  $k_z = 0$  and  $k_z = -0.05\frac{\pi}{d}$ , respectively, where the blue lines denote the surface states.

# Surface state robust against $k_z$ -preserved scattering

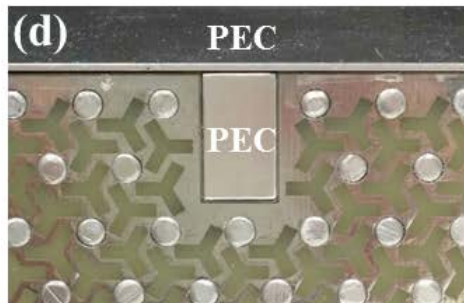
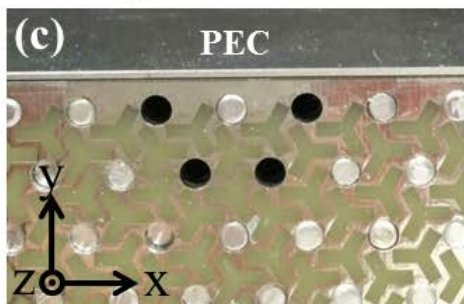
## Simulated field pattern

$$k_z = 0.3\pi/d$$



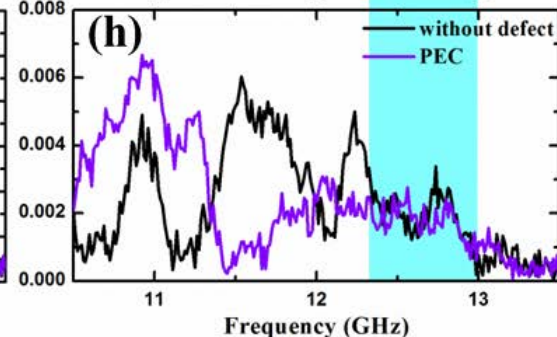
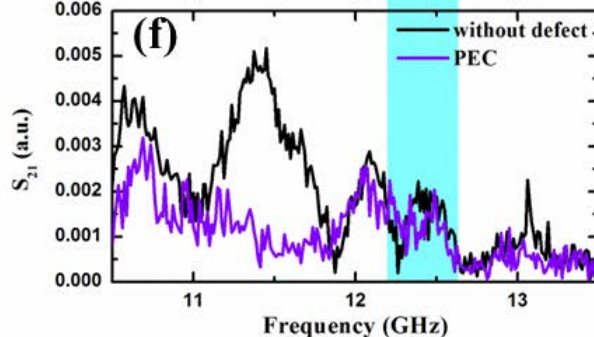
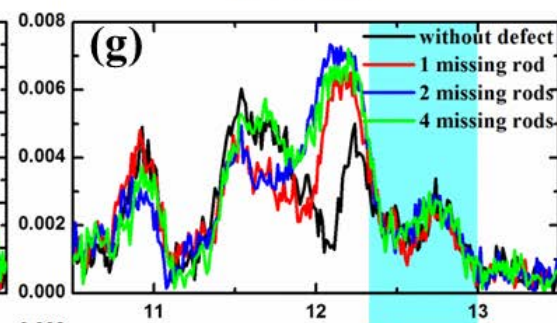
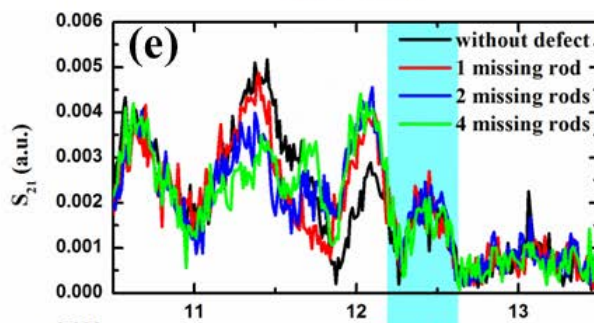
## Measured surface transmission

### Samples with defect

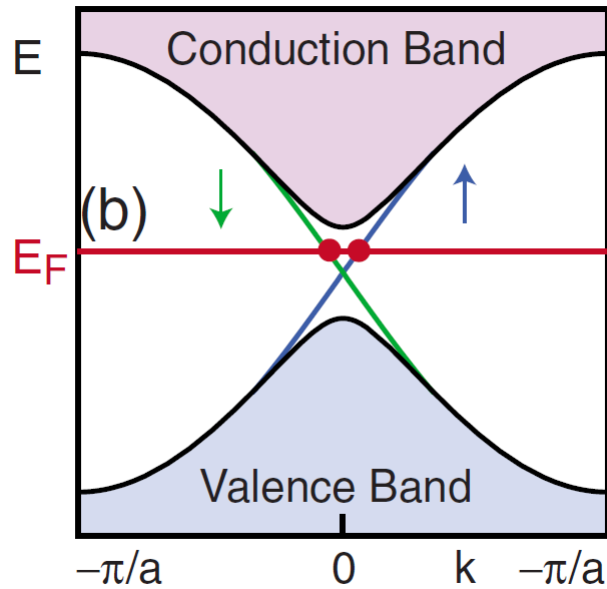


$$\theta = 35^\circ$$

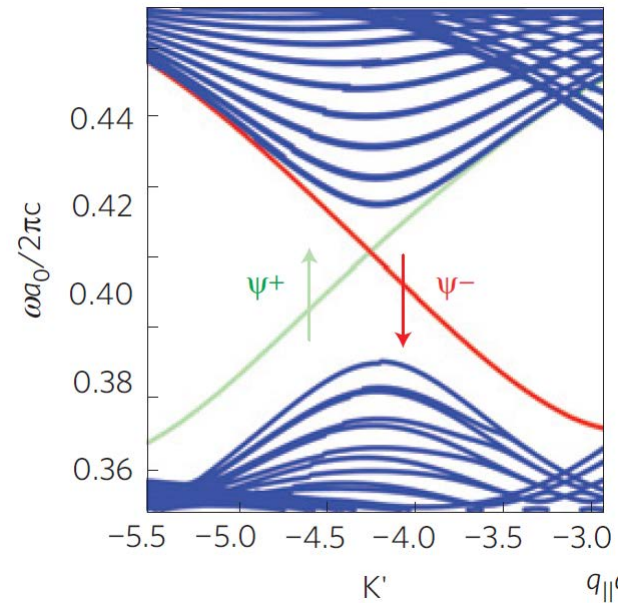
$$\theta = 50^\circ$$



# Symmetry protected transport in a pseudospin-polarized waveguide

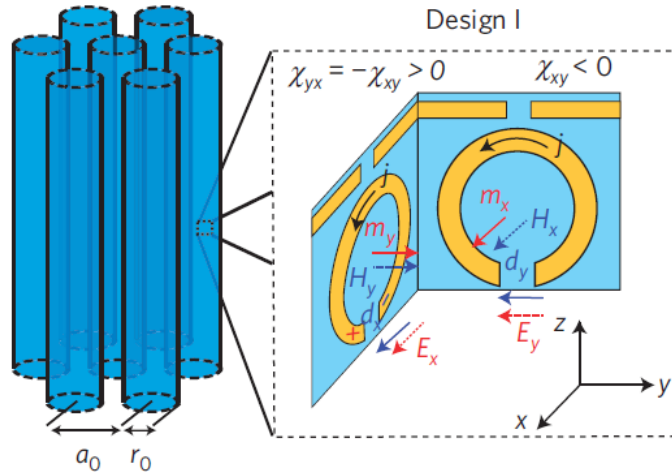


electronic topological insulator



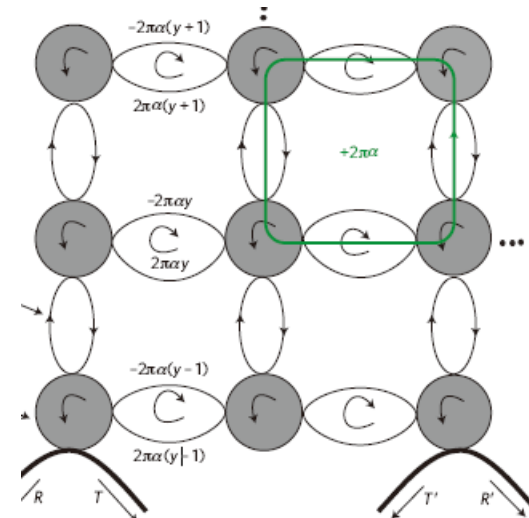
photonic topological insulator

# Spin-filtered edge state of bulk photonic topological insulators



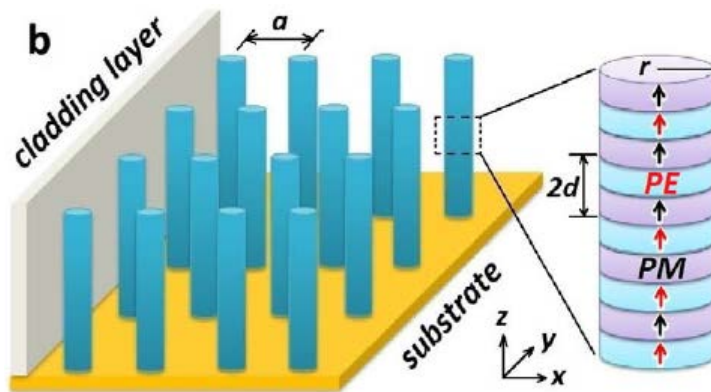
**Bianisotropic metacrystal**

A. B. Khanikaev, S. H. Mousavi, A. H. MacDonald, G. Shvets et.al.  
 Nat. Mater. 12, 233 (2013)



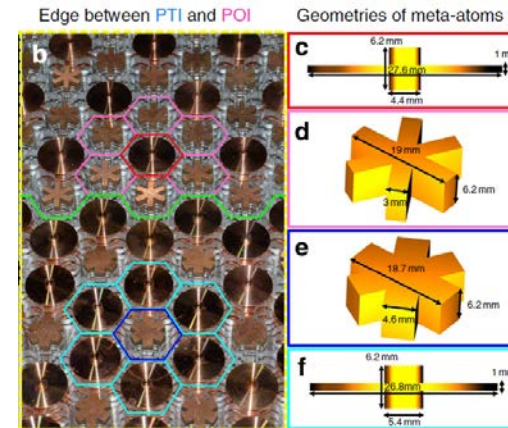
**Coupled resonator optical waveguide**

M. Hafezi, J. M. Taylor et.al.  
 Nat. Phys. 7, 907 (2011); Nat. Photon. 7, 1001 (2013)



**Piezoelectric and piezomagnetic superlattice**

C. He, X.-C. Sun, X.-P. Liu, M.-H. Lu, Y. Chen, L. Feng,  
 and Y.-F. Chen, arXiv:1405.2869



**Metacrystal in planar waveguide**

W.-J. Chen, J.-W. Dong, C. T. Chan et. al. Nat. Comm. 5, 5782 (2014)

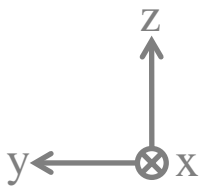
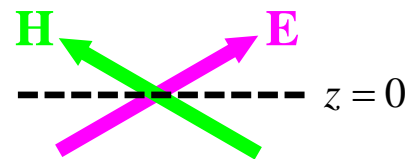
Under the symmetry of  $\epsilon(x, y, z) = \mu(x, y, -z)$ , Maxwell equations can be reduced to two decoupled equations for two pseudo spins.

$$\begin{pmatrix} J_x(z) \mp M_x(-z) \\ J_y(z) \mp M_y(-z) \\ J_z(z) \pm M_z(-z) \end{pmatrix} = i\omega\epsilon(z)\Psi_{\pm}(z) \pm \begin{pmatrix} 0 & \partial_z & \partial_y \\ -\partial_z & 0 & -\partial_x \\ \partial_y & -\partial_x & 0 \end{pmatrix} \Psi_{\pm}(-z)$$

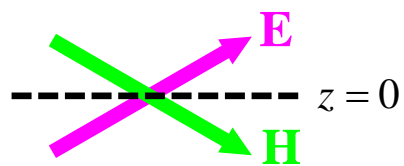
$$\Psi_+(z) = \begin{pmatrix} E_x(x, y, z) - H_x(x, y, -z) \\ E_y(x, y, z) - H_y(x, y, -z) \\ E_z(x, y, z) + H_z(x, y, -z) \end{pmatrix} \longleftrightarrow \Psi_-(z) = \begin{pmatrix} E_x(x, y, z) + H_x(x, y, -z) \\ E_y(x, y, z) + H_y(x, y, -z) \\ E_z(x, y, z) - H_z(x, y, -z) \end{pmatrix}$$

**time reversal**  
**(E → E\*, H → -H\*)**

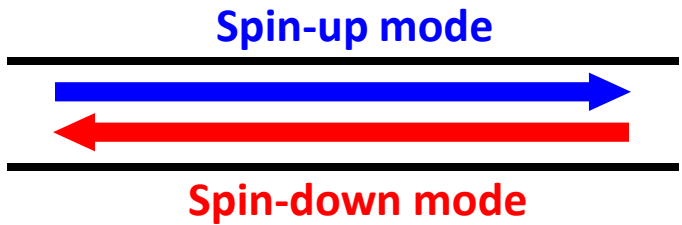
**Pseudo spin-up** ( $\bar{H} = -\sigma_z \bar{E}$ )



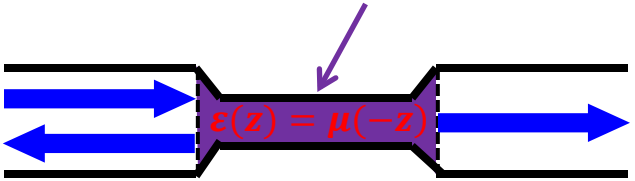
**Pseudo spin-down** ( $\bar{H} = \sigma_z \bar{E}$ )



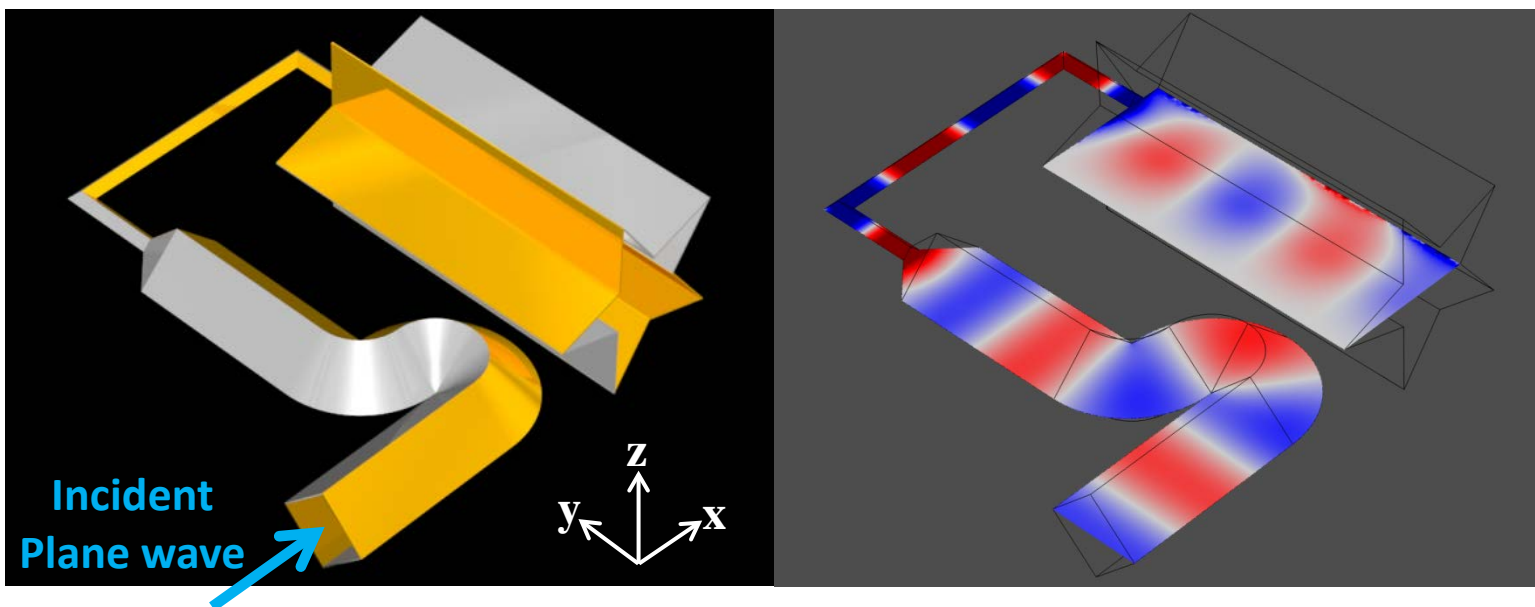
Symmetry protected transport in **spin-filtered channel**



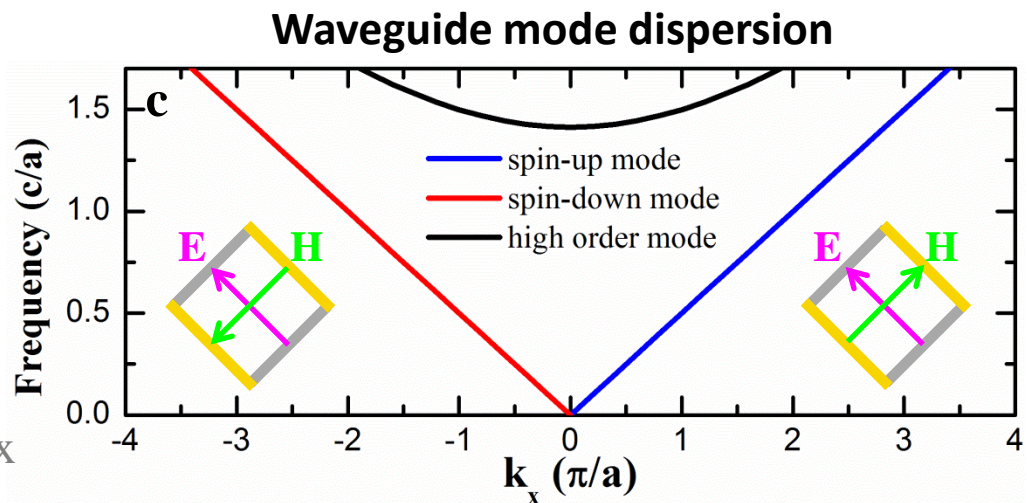
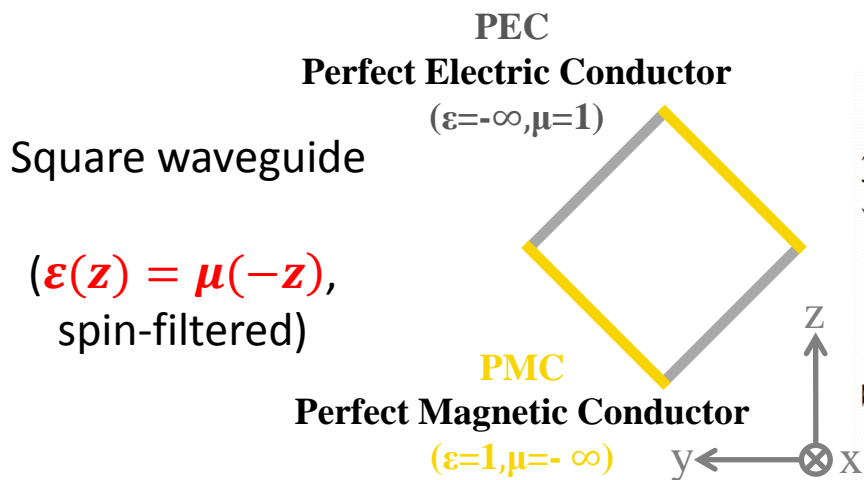
$\epsilon$ - $\mu$  symmetric deformation



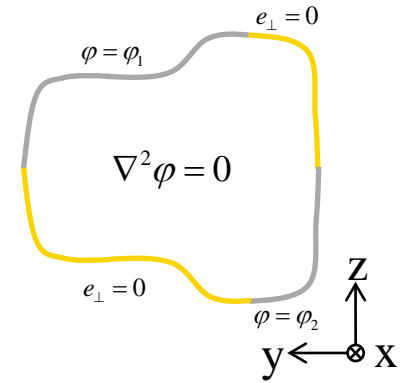
Robust against  $\epsilon$ - $\mu$  symmetric deformation



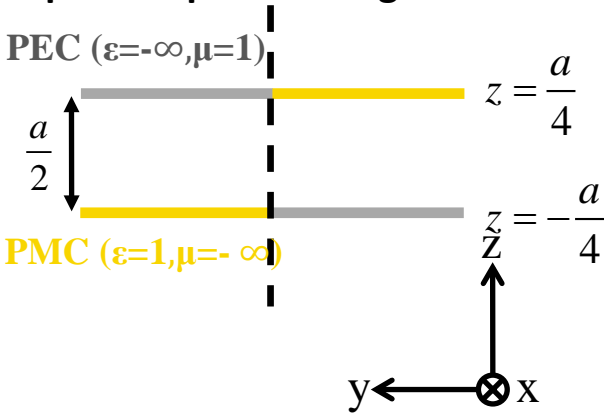
## Spin-filtered channel by applying $\epsilon$ - $\mu$ symmetric boundary conditions



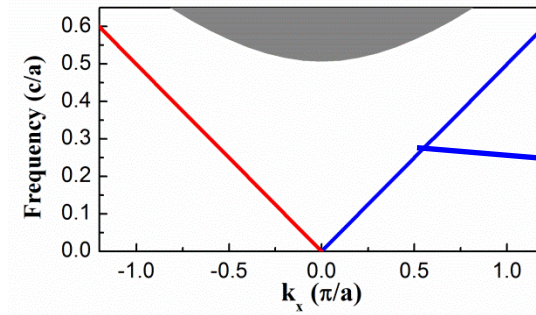
Spin-filtered feature of the PEC PMC waveguide do not rely on the shape of boundaries, but the  $\epsilon$ - $\mu$  symmetry.



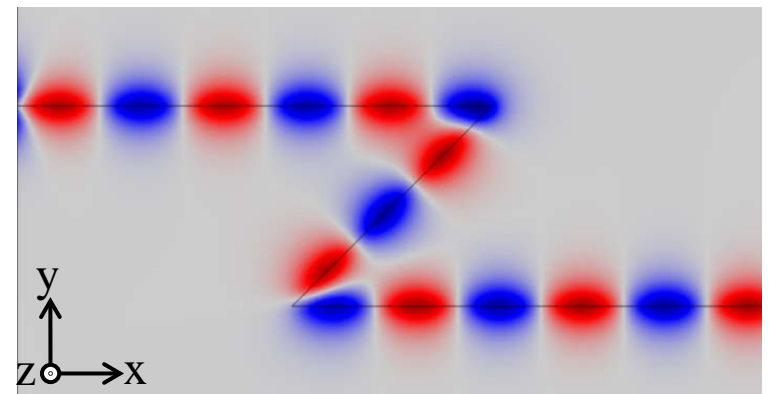
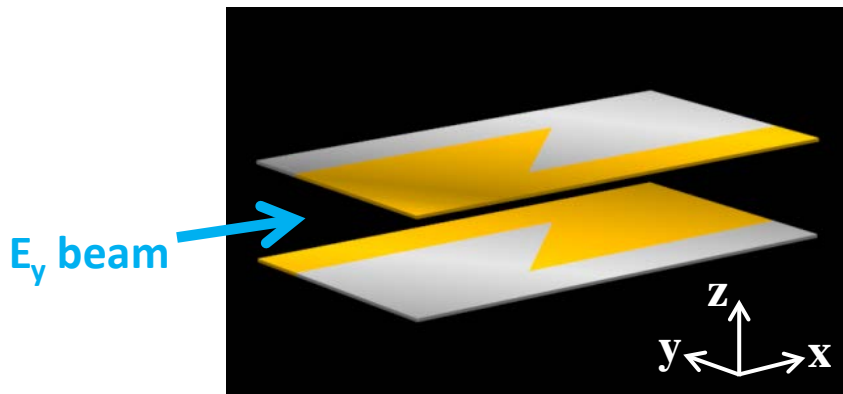
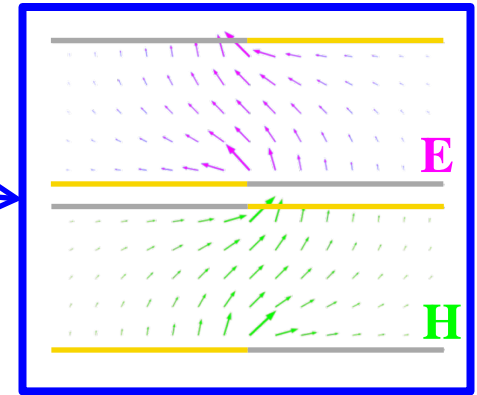
Edge between two parallel plate waveguides



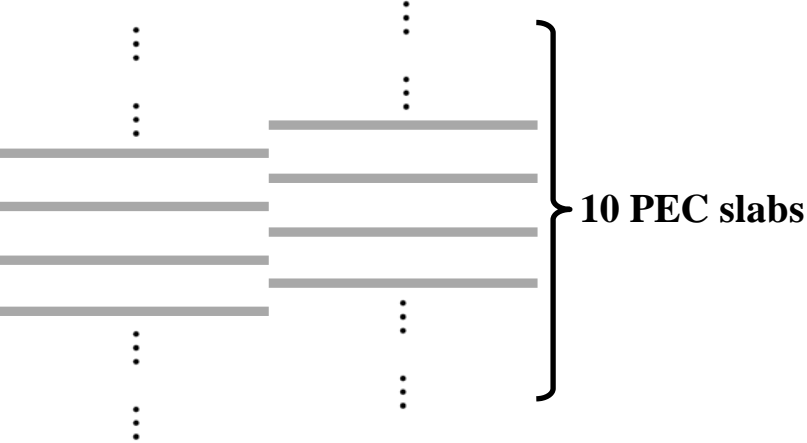
Edge mode dispersion



Eigen **E**/**H** field of forward edge mode



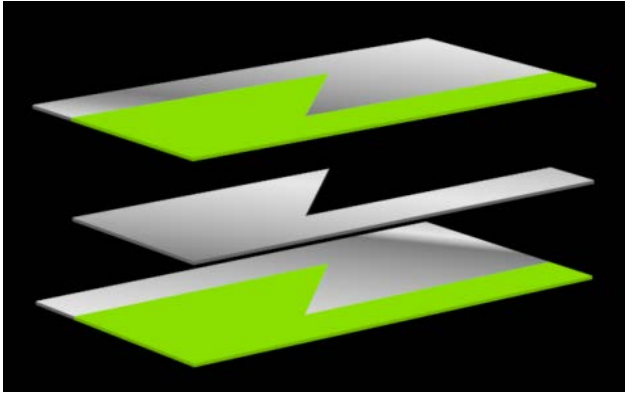
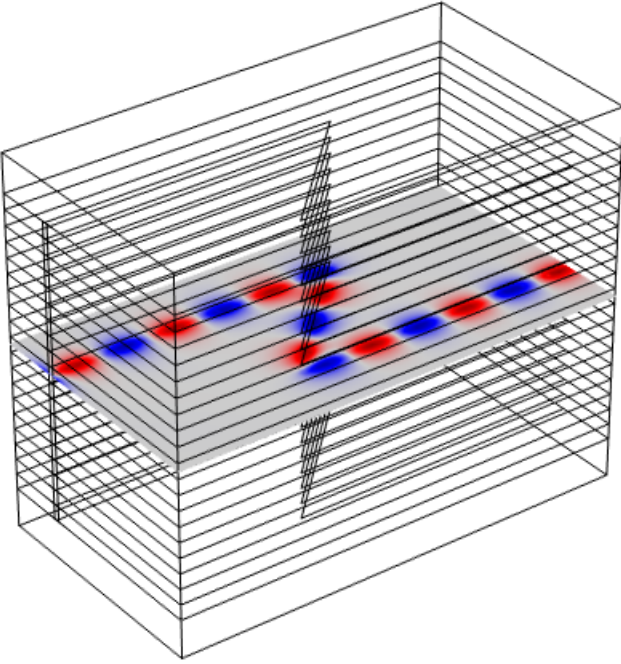
PMC can only be realized for a single frequency. To achieve broad bandwidth, we propose the periodic structure without PMC.



**Fully symmetric solution**

$$\begin{array}{l}
 E_x(x, y, z) \quad E_y(x, y, z) \quad E_z(x, y, z) \\
 H_x(x, y, z) \quad H_y(x, y, z) \quad H_z(x, y, z) \\
 \cdots \\
 E_x(-z - \frac{a}{2}) \quad E_y(-z - \frac{a}{2}) \quad -E_z(-z - \frac{a}{2}) \\
 -H_x(-z - \frac{a}{2}) \quad -H_y(-z - \frac{a}{2}) \quad H_z(-z - \frac{a}{2})
 \end{array}$$

Periodic boundary



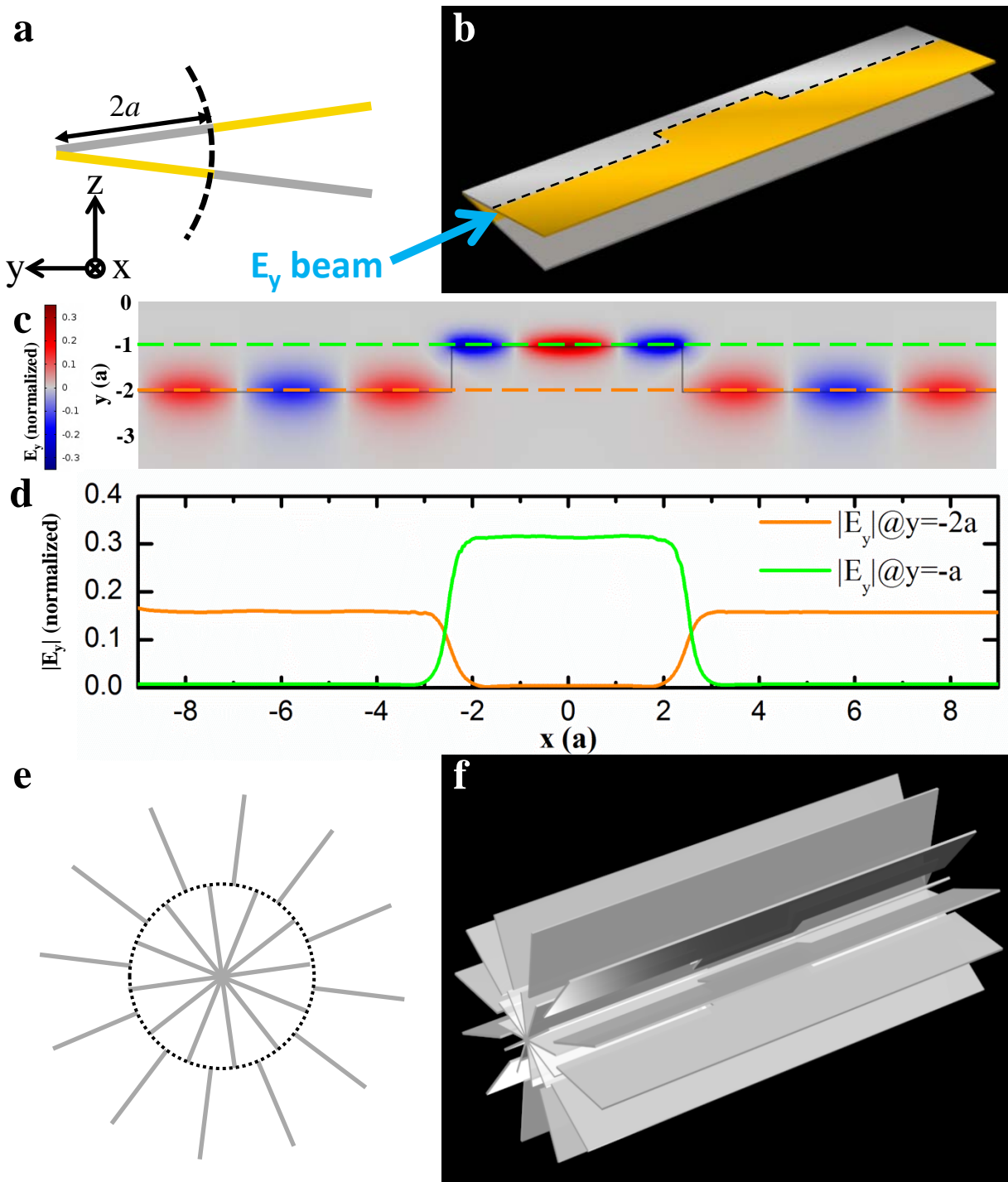


**Figure 4 | Field concentrator with broad bandwidth.** (a) Cross-sectional view of an edge (black dashed line) between two fan-shaped plate waveguides. The distance between the apex and the edge is  $2a$ . (b) Oblique view of a zigzag edge whose middle part is shifted closer ( $1a$ ) to the apex. (c) field pattern of the zigzag edge shown in (b) normalized by the incident field amplitude. When the EM wave is launched from the left, it travels through the shifted part without backscattering, which is verified by comparing the field amplitudes on the left- and right-hand sides. (d) Electric field amplitudes at the orange and green dashed lines in (c), showing that the field amplitudes in the middle shifted edge region are doubled, as required by energy flux conservation. The edge between two fan-shaped plate waveguides can also be realized in the structure shown in (e), which is periodic in the azimuthal direction. (f) Oblique view of a field concentrator built from PEC slabs.

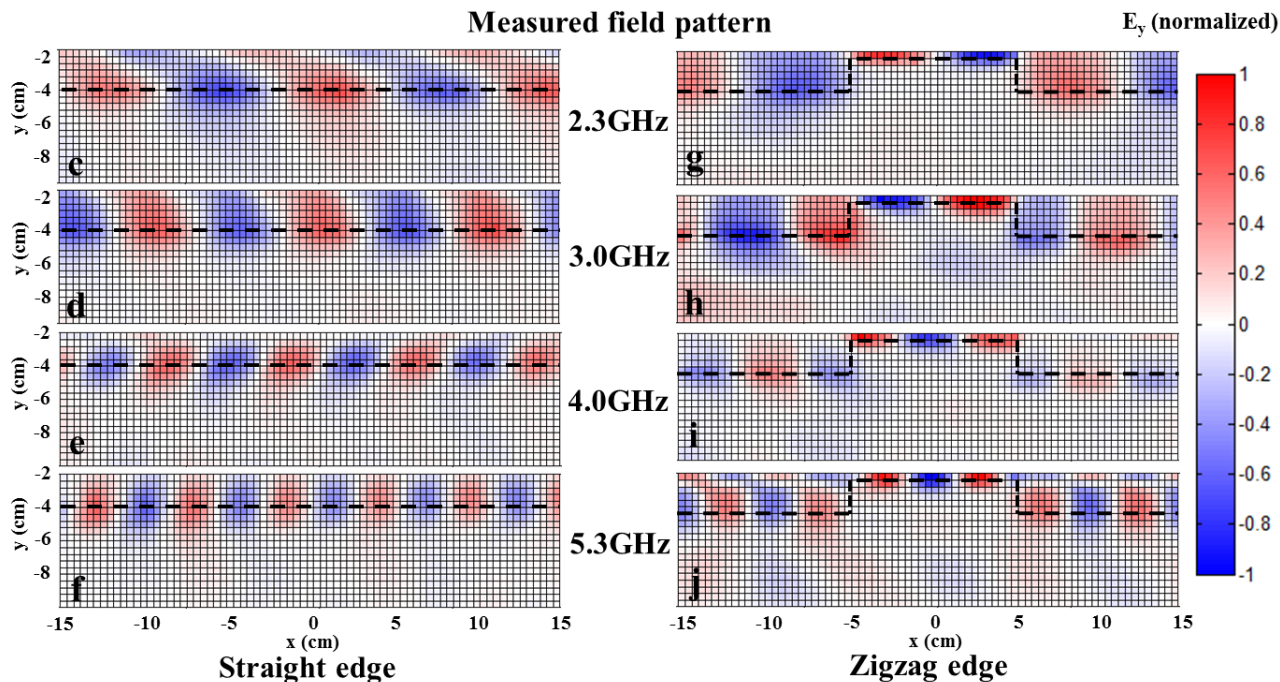
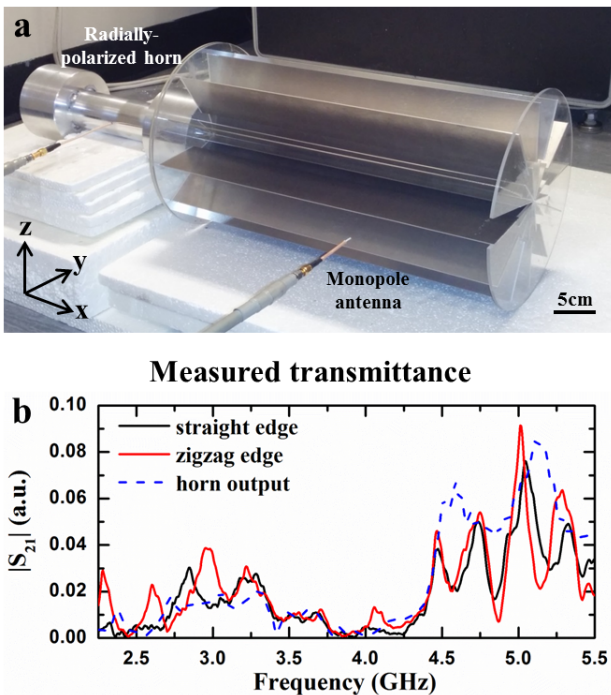


**Figure 5 | Experimental demonstration of a pseudospin-polarized waveguide.** (a) The experimental setup. EM wave was emitted from a radially-polarized horn on the left of the sample. The electric field inside the sample was measured with a monopole antenna mounted on a stepmotor. (b) Measured transmittance of the sample with a straight edge (black line) or a zigzag edge (red line). The shifted region in the zigzag edge did not introduce obvious backscattering. Robust transport was also demonstrated by the measured field patterns. (c-f) Measured fields in the sample with straight edges at 2.3, 3.0, 4.0 and 5.3 GHz. (g-j) Measured fields in the sample with zigzag edge. Black dashed lines highlight the locations of edges. EM waves were always guided along the straight or zigzag edge. The field amplitudes on the left and right of the zigzag edge are almost the same, demonstrating one-way transport. The fields in the shifted region were enhanced, compared to the unshifted region. The measured field patterns at each frequency are normalized by the maximal amplitude in the zigzag edge.

**Thank you for your attention!**